REGULAR ARTICLE

Atomic carbon adsorption on Ni nanoclusters: a DFT study

Qiang Wang · Kok Hwa Lim · Shuo-Wang Yang ·
Yanhui Yang · Yuan Chen

Abstract Atomic carbon is a key intermediate interacting with transition metal clusters during the growth of carbon nanotube (CNT). Present density functional calculations studied the initial carbon adsorption on four Ni nanoclusters (N_{13}, N_{15}, N_{38}, and N_{55}). Our results show that carbon atoms preferentially adsorb on high-coordination sites, and carbon adsorption energies are larger on smaller Ni clusters. Ni cluster reconstruction plays an important role in creating more stable subsurface adsorption sites. The migration of adsorbed carbon atom on the surface threefold hollow site into the underlying interstitial subsurface positions is thermodynamically and kinetically feasible. The results indicate that the investigation of CNT growth mechanism should include both surface and subsurface carbon atoms, coupled with surface reconstruction of Ni nanoclusters.

Keywords Carbon adsorption · Ni · Nanocluster · Carbon nanotube · Growth mechanism

Q. Wang · K. H. Lim (✉) · Y. Yang · Y. Chen (✉)
School of Chemical and Biomedical Engineering,
Nanyang Technological University, 62 Nanyang Drive,
Singapore 637459, Singapore
e-mail: kokhwa@ntu.edu.sg

Y. Chen
e-mail: chenyuan@ntu.edu.sg

S.-W. Yang
Institute of High Performance Computing (IHPC),
1 Fusionopolis, Way, #16-16 Connexis,
Singapore 138632, Singapore

1 Introduction

Carbon nanotubes (CNTs) have evolved into one of the most intensively studied materials in the past decade due to their intriguing properties [1, 2]. However, experimental methodology is still inadequate to gain a reliable control of CNT synthesis due to the limited understanding on CNT growth mechanism. C atoms are commonly generated from the decomposition/evaporation of gas/solid phase carbon precursors in different CNT synthesis methods [3–8]. It is generally accepted that the adsorption of C atoms (or dimers) on metal nanoparticles is an initial step in the CNT growth. Subsequently, the diffusion of adsorbed C atoms on/in metal clusters controls the CNT cap nucleation, eventually resulting in the growth of CNTs [9–11]. The interaction between growing carbon structures and metal clusters would determine the CNT diameter [12, 13] and chirality [14, 15]. Adding to the complication, experimental studies also found that the dynamic reshaping of catalyst nanoparticles occurs during the CNT growth [16]. CNT researchers are puzzled by a number of problems existing at the initial CNT growth step, C atom adsorption on metal nanoparticles. The metal nanoparticles around 1 nm in diameter are specially important, because they are responsible to the single-walled carbon nanotubes (SWCNTs) structure control [17]. It is necessary to answer the following questions: (1) are there significant differences in the C atom adsorption energy on metal nanoparticles of different sizes? (2) Would C atoms preferably adsorb on specific facets of a metal nanocluster? (3) Whether adsorbed C atoms can penetrate metal clusters or merely stay on the cluster surface?

Many unsolved puzzles in the CNT growth are difficult to be elucidated experimentally. Ab initio modeling offers a powerful alternative. Previously, the adsorption of

carbon on Ni surfaces has been studied theoretically to understand the catalytic hydrocarbon synthesis. In the early ab initio calculations, due to the limitation of computational capacity, fixed Ni cluster models arranged according to the geometry of low index Ni surfaces were employed [18–21]. Without considering the reconstruction of Ni atoms, the obtained C absorption energy on these Ni surfaces is usually over predicted. Zhang et al. [22] extended the calculation to Ni periodic slabs of three low-index Ni surfaces. Furthermore, C adsorption on a Ni_{38} cluster was also reported [22]. Several other recent ab initio calculations studied the C adsorption and diffusion on the surface and in the subsurface of periodic slabs of Ni(111), Ni(100), and Ni bulk [23–25]. Their results suggested that C can diffuse on Ni surfaces, as well as into the subsurface sites before forming metal carbides [23–25]. It would be interesting to evaluate whether the similar phenomena also happen on small Ni nanoclusters with the size of about 1 nm, which are the catalysts usually employed in SWCNT growth.

In the present work, we revisited the adsorption of C atoms on a series of Ni metal nanoclusters using density functional calculations to address the aforementioned three C adsorption questions related to CNT growth. (1) The effect of Ni cluster size. Experimental results found that a small change in catalyst particle diameter has a significant impact on the diameter and chirality of CNTs produced [13]. (2) The role of Ni nanoparticle facets. A previous calculation has suggested that C adsorption energy may be distinct on various facets of the Ni_{38} cluster [22]. In this study, we extended our calculations to nanoclusters with four different sizes. (3) To answer the intriguing question: whether a C atom can enter a small nanocluster or only preferentially adsorbs on its surface. A series of Ni nanoclusters were modeled. Adsorption sites on individual cluster facets, along with conceivable subsurface adsorption sites were investigated. The adsorption energy, surface reconstruction, and charge distribution induced by C absorption were compared. The possibility of C migrating into the bulk of Ni nanocluster was evaluated by studying the stability of C atoms at subsurface sites. The transition states of C diffusion were also identified. These results would lead to a better understanding of the CNT growth mechanism,

2 Computational methodology

Four nanoclusters, namely Ni_{13}, Ni_{15}, Ni_{38}, and Ni_{55} (illustrated in Fig. 1), were modeled based on a simulated annealing study on the structure stability of $Ni_{2–55}$ [26] and an experimental electric dipole polarizability study for $Ni_{12–58}$ [27]. These nanoclusters are in the diameter range suitable for SWCNT growth. Three types of high symmetry
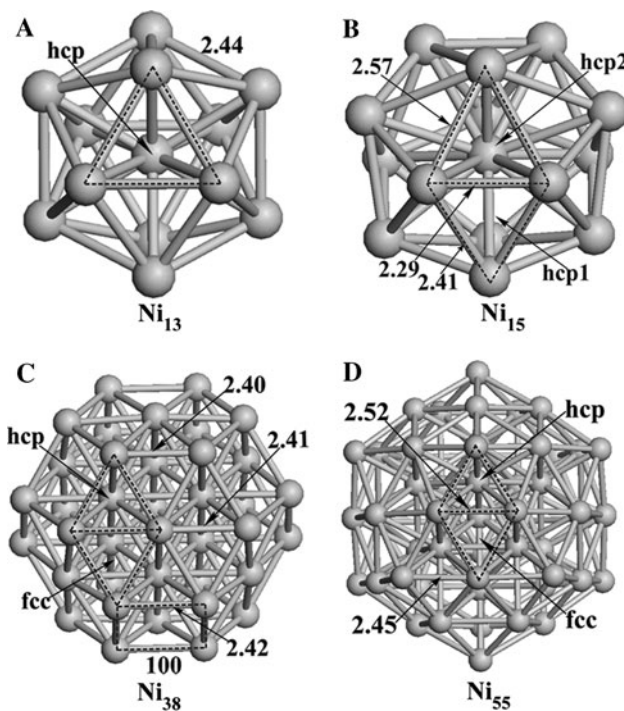
Fig. 1 Ni clusters: a Ni_{13}, b Ni_{15}, c Ni_{38}, and d Ni_{55}. Surface adsorption sites are depicted on the models with Ni–Ni bond lengths showed in angstroms

surface adsorption sites were investigated, including one fourfold hollow site (μ_4-100) on (100) facets and 2 three-fold hollow fcc or hcp sites (μ_3-fcc, μ_3-hcp) on (111) facets. At the same time, several subsurface sites in nanoclusters were also investigated (Fig. 2). Here, we restricted our report to the most stable C adsorption sites. Two types of cluster models were studied including (1) the fixed models, in which Ni atoms were fixed at their optimized locations and (2) the relaxed models, in which the locations of Ni atoms were fully optimized with the C adsorbate. The relaxed models allow us to investigate the reconstruction of clusters upon C adsorption. Our initial intention is to evaluate whether there are significant differences in term of C adsorption energies between the fixed and relaxed models. In general, fixed models require much less computational time. We speculated that if no noticeable differences are observed between the two types of models, then the fixed models could be considered for our further studies, such as C diffusion and CNT cap nucleation on metal cluster surfaces. Furthermore, the activation barriers of C surface-to-subsurface diffusion were determined by scanning the potential energy profiles (PEPs) along the lines, which connect the local energy minima of C atoms adsorbed at the surface fcc sites and subsurface μ_6-sub sites for Ni_{38} clusters (Fig. 3). For each sampling point, the nearest neighbor Ni atoms of a C adsorbate were relaxed, while the radial distance of the C atom and other Ni atoms
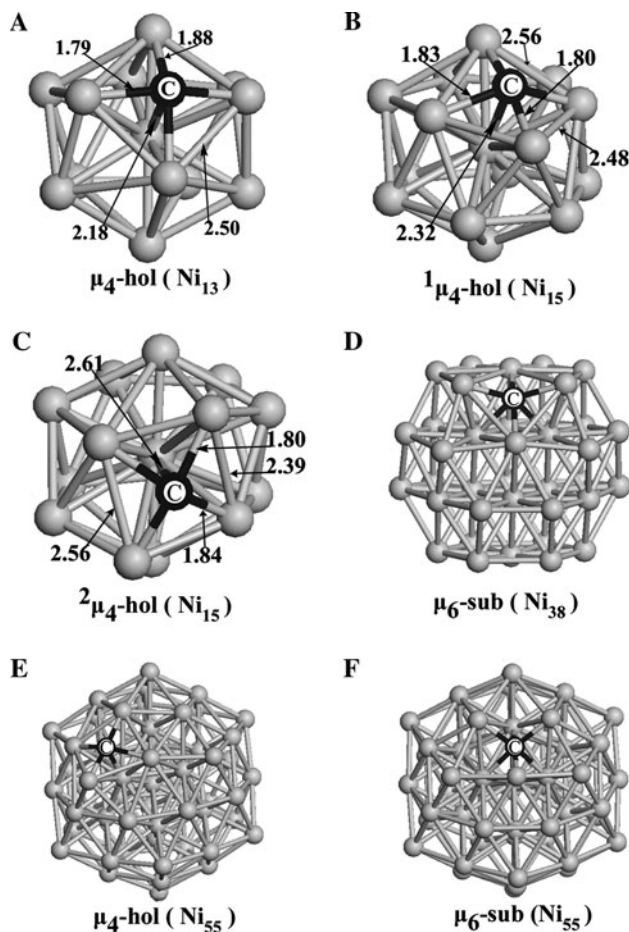
Fig. 2 Subsurface adsorption sites: **a** μ_4-hol (Ni$_{13}$), **b** $^1\mu_4$-hol (Ni$_{15}$), **c** $^2\mu_4$-hol (Ni$_{15}$), **d** μ_6-sub (Ni$_{38}$), **e** μ_4-hol (Ni$_{55}$), and **f** μ_6-sub (Ni$_{55}$). Subsurface adsorption sites are depicted on the models with Ni–Ni bond lengths showed in angstroms

Fig. 3 Potential energy profiles from an fcc threefold hollow surface site to a sixfold subsurface site on a Ni$_{38}$ cluster. Two local minimums on the curves correspond to fcc threefold hollow sites (on the *right*) and octahedral subsurface holes (on the *left*). $R_{C\text{-cen}}$: interatomic distances between an adsorbed C atom and Ni atoms at the center of the cluster

were fixed. To validate the transition state found by the PEP method, a precise nudge elastic band (NEB) method was also applied to locate the transition-state structure of the surface-to-subsurface diffusion [28].

All computations were performed spin polarized, with the Perdew–Burke–Ernzerhof (PBE) exchange correlation function [29] using the VASP code [30, 31]. The interactions between an atomic core and electrons were described by the projector augmented wave method [32, 33]. The plane-wave basis set energy cutoff was set to 400 eV. The periodic boundary conditions were implemented with at least 1 nm vacuum to preclude interactions between a cluster and its images (using cubic supercells with one side of 15 Å for the smaller Ni$_{13}$ and Ni$_{15}$ and 20 Å for the bigger Ni$_{38}$ and Ni$_{55}$ clusters). Because the discrete character of the Ni clusters, the reciprocal space integration was performed with a $1 \times 1 \times 1$ k-point mesh. Between spin-polarized and non-spin-polarized calculations performed on the Ni$_{13}$ system, the spin-polarized calculations show higher-binding energies of adsorbed C atoms by ~ 0.3 eV.

Thus, all computations were performed spin polarized for this work. In the current work, we did not further study the magnetization of Ni cluster, as Ni could be considered as a weakly magnetic material at 0 K, according to the work by Reddy et al. [34]. All local minimums and transition states were verified by frequency analysis. The Ni$_2$ dimer with a cubic supercell of 15^3 Å^3 in size and Ni bulk were also calculated using the optimized lattice constant as references to the results obtained on four Ni clusters. Charge distribution was calculated by the Bader charge analysis [35, 36].

The average binding energy per Ni atom of four clusters was calculated according to Eq. 1, where n is the number of Ni atoms per cluster.

$$E_b(\text{Ni}_n) = [nE(\text{Ni atom}) - E(\text{Ni}_n)]/n \qquad (1)$$

From the total energy of C adsorbed clusters $E_{tot}(\text{C/Ni}_n)$, the total energy of pure clusters $E_{tot}(\text{Ni}_n)$, and the energy of free C atoms $E_{tot}(\text{C atom})$, binding energies per C atom E_b can be calculated according to Eq. 2, where n is the number of Ni atoms per cluster.

$$E_b = E_{tot}(\text{Ni}_n) + E_{tot}(\text{C atom}) - E_{tot}(\text{C/Ni}_n). \qquad (2)$$

Table 1 Calculated results of the average binding energy E_b (eV), the average coordination number Z, bond lengths to the central Ni atom R_{Ni-Cen} (Å), and surface bond lengths R_{Ni-Ni} (Å)

	Ni$_2$	Ni$_{13}$	Ni$_{15}$	Ni$_{38}$	Ni$_{55}$	Ni-bulk
E_b	2.23	3.22	3.26	3.75	3.92	4.08
Z	1	5.5	5.7	7.2	7.7	12
R_{Ni-Cen}		2.32	2.22, 2.51	1.74, 3.08, 3.81	2.36, 4.65, 4.07	
R_{Ni-Ni}	2.09	2.44	2.29, 2.41, 2.57	2.40, 2.41, 2.42	2.45, 2.52	2.49

The average coordination number Z is calculated based on Knickelbein [38]

3 Results and discussion

3.1 Ni$_n$ (n = 13, 15, 38, and 55) clusters

Figure 1 illustrates the optimized structures of four Ni clusters. Ni$_{38}$ has a truncated octahedral geometry; Ni$_{15}$ has a hexagonal antiprism structure; Ni$_{13}$ and Ni$_{55}$ adopt an icosahedral geometry. Their geometries are similar to those from a previous report for the Pt$_n$ (with n = 13, 38 and 55) nanoclusters [37]. The calculated average binding energies and Ni–Ni bond lengths of these four clusters are listed in Table 1.

Ni$_{13}$ has one atom at the center and other 12 identical atoms on the spherical shell surface with a coordination number of 6. The distance between the spherical shell and the central atom is 2.32 Å. The surface Ni–Ni bond length is 2.44 Å. Ni$_{15}$ has three atoms along the symmetric axis. Similar to Ni$_{13}$, it has only one atom at the center, and all other Ni atoms are on the surface. Radial distribution analysis shows that there are two types of non-equivalent Ni atoms relating to the center atom. Their distances to the central atom are 2.22 and 2.51 Å, and their coordination numbers are 6 and 7, respectively. The bond lengths between two Ni atoms at the Ni$_{15}$ surface are 2.29, 2.41, and 2.57 Å (see Fig. 1b for illustration), which are in the range of the bond lengths for bulk Ni (2.49 Å) and dimer Ni$_2$ (2.09 Å).

Radial distribution analysis shows that Ni atoms in the optimized structure of Ni$_{38}$ can be classified into three types of non-equivalent atoms related to the center of Ni$_{38}$. The first group has six identical atoms in the inner shell, which are 1.74 Å to the center. They have an octahedral arrangement. The second group has 24 identical atoms lying at the vertexes of six (100) faces in the outer shell. They have a coordination number of 6, and are 3.81 Å to the cluster center (denoted as "edge atoms"). The third group contains eight atoms of the outer shell. They lie at the center of the eight (111) faces. They have a coordination number of nine, and are 3.08 Å to the Ni$_{38}$ cluster center (denoted as "center atom") (see Fig. 1c). The surface bond lengths are 2.40–2.42 Å between two surface Ni atoms.

Based on the Ni$_{13}$ icosahedral structure, the Ni$_{55}$ is built by adding 30 atoms on the top of Ni$_{13}$ "edge atoms" with a coordination number of 8 (denoted as "edge atoms" for

Ni$_{55}$), and additional 12 atoms on the top of Ni$_{13}$ vertex positions with a coordination number of 6 (denoted as "top atoms" for Ni$_{55}$). The "top atoms" are 4.65 Å away to the cluster center, while the "edge atoms" are 4.07 Å to the cluster center. The surface bond lengths are 2.52 Å between two "edge atoms" and 2.45 Å for two adjacent "top atom" and "edge atom" (illustrated in Fig. 1d). Furthermore, a Ni$_{55}$ sublayer is 2.36 Å to the cluster center, suggesting this layer is slightly enlarged compared to the original Ni$_{13}$ clusters, due to addition of surface atoms.

Table 1 shows that the average binding energies and average coordination numbers increase with the increase of Ni cluster size. The minimum Ni–Ni binding energy (3.22 eV for Ni$_{13}$) is higher than the binding energy of a Ni$_2$ dimmer (2.23 eV), and the strongest Ni–Ni binding energy (3.92 eV for Ni$_{55}$) is lower than the cohesive energy of the bulk Ni (4.08 eV). The average interatomic distance also increases with the increase of the Ni cluster size, varying between the bond distance of Ni$_2$ dimer (2.09 Å) and bulk Ni (2.49 Å). Our simulation results are also consistent with the structural data obtained from an extended X-ray absorption fine structure (EXAFS) experiment [39].

3.2 C adsorption on Ni$_n$ (n = 13, 15, 38, and 55)

Table 2 summarizes our results of C adsorption on Ni clusters. The adsorption energy, interatomic distance, and charge distribution induced by C absorption on different sites were first studied using fixed Ni clusters as described in Sect. 3.2.1. Next, the effect of Ni cluster relaxation on the C adsorption energies and bond lengths was further investigated using fully relaxed Ni clusters. Lastly, the stability of C atoms at subsurface sites in relaxed Ni clusters was investigated to evaluate the possibility of C penetration into the clusters.

3.2.1 C adsorption on fixed Ni$_n$ clusters

When C is adsorbed on Ni$_{13}$, only the hcp (μ_3-hcp) adsorption site is stable with adsorption energy of 7.06 eV. Two stable threefold hollow adsorption sites are found on the Ni$_{15}$ instead, which consist of three Ni atoms with

Table 2 Observables calculated for the adsorption of C atoms on threefold sites (μ_3-fcc, μ_3-hcp), fourfold sites (μ_4-100)), subsurface fourfold hollow sites (μ_4-hol), and sixfold hollow sites (μ_6-sub) on both fixed and fully relaxed Ni$_n$ (with n = 13, 15, 38, and 55) clusters

Sites		Ni$_{13}$		Ni$_{15}$		Ni$_{38}$		Ni$_{55}$	
		Fixed	Relaxed	Fixed	Relaxed	Fixed	Relaxed	Fixed	Relaxed
E(eV)	μ_3-fcc					6.98	7.17	6.80	6.94
	μ_3-hcp	7.06	7.29	7.19[a], 7.16[b]	7.37	6.95	7.25	6.89	7.09
	μ_4-100					7.82	8.02		
	μ_4-hol		7.44		8.17[a], 7.92[b]		7.70		7.34
	μ_6-sub								7.41
$R_{\text{C–Ni}}$(Å)	μ_3-fcc					1.77, 1.78	1.76, 1.78	1.79	1.78
	μ_3-hcp	1.77	1.76	1.76[a], 1.78[b]	1.75, 1.77	1.77, 1.76	1.77, 1.75	1.77, 2.94	1.75, 1.76, 2.80
	μ_4-100					1.83	1.83		
	μ_4-hol		1.79, 1.88		1.82				1.76, 1.78, 1.94, 1.98
	μ_6-sub						1.82, 2.08, 1.86		1.82, 1.92
$R_{\text{Ni–Ni}}$(Å)	μ_3-fcc					2.40	2.52, 2.60	2.52	2.56
	μ_3-hcp	2.44	2.61	2.29[a], 2.41[a], 2.29[b], 2.57[b]	2.37, 2.59	2.41	2.62, 2.71	2.45, 2.52	2.65, 2.68
	μ_4-100					2.42	2.54		
	μ_4-hol		2.50		2.48[a], 2.56[a], 2.39[b], 2.56[b]				2.55, 2.73
	μ_6-sub						2.56, 2.68, 2.37, 3.42, 2.44		2.56, 2.52, 2.84

E: adsorption energy of C atoms; $R_{\text{C–Ni}}$: interatomic distances between an adsorbed C atom and its nearest-neighbor Ni atoms; $R_{\text{Ni–Ni}}$: interatomic distances between the two nearest-neighbor Ni atoms

[a], [b] Refer to two different positions on the hcp site shown in Fig. 1

different coordination numbers (denoted as hcp1 and hcp2 in Fig. 1b). However, C adsorption energies on these two sites are similar, 7.19 and 7.16 eV at $^1\mu_3$-hcp and $^2\mu_3$-hcp, respectively. Three stable C adsorption sites are found on Ni_{38} (Fig. 1c). One is the fourfold hollow site (μ_4-100) on the (100) facet with a coordination of four Ni atoms. The others are 2 threefold sites (μ_3-fcc and μ_3-hcp) on the (111) facet. C adsorption on the μ_4-100 site has the highest adsorption energy at 7.82 eV. The adsorption energies on the μ_3-fcc and μ_3-hcp sites are 6.98 and 6.95 eV, respectively. Our results on the Ni_{38} cluster agree with previous reports that atomic C has no preference toward threefold hollow sites on transition metal surfaces, such as the Pd (111) surface [40–42] and Pd nanoclusters [43]. On the other hand, the higher C adsorption energy at the fourfold (μ_4-100) site suggests that C would preferably adsorb on a higher-coordination site of Ni surfaces. Furthermore, two stable adsorption sites are found on Ni_{55}. They are highly symmetric threefold hollow sites, μ_3-fcc and μ_3-hcp (Fig. 1d). C adsorption on the μ_3-fcc and μ_3-hcp sites has adsorption energies at 6.80 and 6.89 eV, respectively. The energy variation between the μ_3-fcc and μ_3-hcp sites may be due to the local environment differences of these two sites. Shown in Fig. 1, Ni atoms forming the μ_3-hcp site have a coordination number of 6, while Ni atoms forming the μ_3-fcc site have a coordination number of 8. Overall, our investigation of C adsorption energies on fixed clusters shows two trends: (1) C atoms prefer adsorbing on highly coordinated sites, such as μ_4-100, μ_3-hcp, and μ_3-fcc. (2) C adsorption is stronger on smaller clusters. For example, the adsorption energies increase from 6.89 eV (Ni_{55}) to 7.19 eV (Ni_{15}) on the μ_3-hcp site, and from 6.80 to 6.98 eV (Ni_{38}) on the μ_3-fcc site.

In addition to the adsorption energies, Table 2 also shows the interatomic distances between adsorbed C atoms and their nearest-neighbor Ni atoms ($R_{C–Ni}$). The $R_{C–Ni}$ is 1.83 Å at the μ_4-100 site. This agrees with previous experimental observations [27, 44]. Overall, the values of $R_{C–Ni}$ have little variation among all adsorption sites on the fixed Ni clusters. Furthermore, the Bader charges of adsorbed C atoms were calculated. The charges of C atoms adsorbed on the μ_3-fcc, μ_3-hcp, and μ_4-100 sites are about −0.78 e, −0.81 e, and −0.96 e, respectively. The negative values indicate that net charges are transferred from the neighbor Ni atoms to the adsorbed C atoms. Unlike the significant differences observed on adsorption energies, the charges of adsorbed C atoms show little variation on four Ni clusters.

3.2.2 C adsorption on relaxed Ni_n clusters

Previously, fixed cluster models were commonly utilized due to the limitation of computational capacity [18–21]. In

our fixed Ni cluster studies, cluster reconstructions upon the adsorption of C atoms were also neglected. Because experimental studies have suggested that metal cluster reconstruction could happen during CNT synthesis [16], the results obtained on fixed models may not be appropriate for investigating the CNT growth mechanism. Thus, fully relaxed Ni cluster models were studied.

Two stable adsorption sites can be identified on the fully relaxed Ni_{13} cluster, in contrast to one stable site found on the fixed Ni_{13} cluster. One site is the μ_3-hcp with a similar geometric configuration as the μ_3-hcp on the fixed cluster. The other is a new hollow site (μ_4-hol) (see Fig. 2a). Our simulation results showed that a C atom adsorbed on a Ni–Ni bridge site can break the Ni–Ni surface bond to increase its coordination number from 3 to 4, resulting in the reconstruction of Ni_{13}. Using single point calculation, we found that the energy required by the Ni_{13} cluster reconstruction is 0.64 eV. This energy may be compensated by the exothermic Ni–C bond formation, leading to a more stable adsorption complex with adsorption energy of −7.44 eV. This adsorption energy (at μ_4-hol) is lower than that at the μ_3-hcp site by 0.15 eV. Furthermore, energy of C adsorption at the μ_3-hcp site on the fully relaxed Ni_{13} cluster is lower by ~0.2 eV, comparing to the adsorption energy at the μ_3-hcp site on the fixed Ni_{13}. Three stable adsorption sites were found on the relaxed Ni_{15} cluster. One is at the μ_3-hcp site. The other two are hollow sites $^1\mu_4$-hol and $^2\mu_4$-hol, and each hollow site is connected with four Ni atoms (Fig. 2b, c). Similar to the μ_4-hol site on Ni_{13}, the two μ_4-hol sites on Ni_{15} originate from the breakdown of Ni–Ni surface bonds (2.41 and 2.51 Å, respectively) upon C adsorption. C adsorption at the $^1\mu_4$-hol site (8.17 eV) is the most favorable site among three adsorption sites on Ni_{15}. On the Ni_{38} cluster, three stable surface adsorption sites were found, including μ_4-100, μ_3-hcp, and μ_3-fcc. The C adsorption energies are 8.02, 7.25, and 7.17 eV, respectively. On the Ni_{55} cluster, two stable surface adsorption sites, μ_3-fcc and μ_3-hcp, were found with the adsorption energies of 6.94 and 7.09 eV, respectively. Furthermore, Table 2 also illustrates that the interatomic distances between an adsorbed C atom and its nearest-neighbor Ni atoms becomes shorter on fully relaxed clusters compared to fixed clusters, in consistent with the stronger C–Ni bond formation. However, no significant differences were found on the Bader charges of adsorbed C atoms at different adsorption sites of relaxed clusters.

Overall, the C adsorption energies derived on fully relaxed clusters in this study are comparable with the experimental results, such as Ni (100) (7.35 eV) and Ni (111) (6.94 eV), obtained on single crystal surfaces by measuring the heat of segregation and vaporization through a thermodynamic cycle [45–47]. Similar to the results

obtained on fixed clusters, C adsorption energies are larger on smaller clusters and highly coordinated sites. More importantly, new C adsorption sites were identified on Ni clusters when cluster reconstruction upon C adsorption was considered. In fact, C adsorption energies on reconstructed sites are higher than those on other sites, suggesting reconstructed sites are more favorable adsorption sites. This finding highlights that some previous studies, which investigated carbon diffusion or CNT cap formation on fixed metal clusters could be inadequate [14, 15]. Metal cluster reconstruction is an indispensable part toward a better understanding of CNT growth mechanism.

3.2.3 C adsorption at subsurface sites

An unsolved puzzle in CNT growth mechanism is whether adsorbed C atoms would enter the metal clusters or merely diffuse on the cluster surfaces. Our investigation on the relaxed Ni clusters suggests that surface Ni–Ni bonds can be broken upon C adsorption. Investigating the stability of C atoms at subsurface sites may help to elucidate this puzzle. For this purpose, the stability of subsurface C atoms in fully relaxed Ni_{38} and Ni_{55} clusters was studied.

We identified two interstitial sites in Ni_{38}: one is located at the subsurface octahedral site (denoted as μ_6-sub); and the other is located at the center octahedral site (denoted as μ_6-cen). Between these two subsurface sites, the μ_6-sub is more stable on the relaxed Ni_{38} cluster (Fig. 2d). The adsorption energy on μ_6-sub site is 0.32 eV less than that of the most stable surface adsorption site (μ_4-100). This may be due to the fact that a C atom at the μ_6-sub subsurface adsorption site is located in a confined space. Two stable C subsurface adsorption sites, μ_4-hol and μ_6-sub, were identified (shown in Fig. 2e and f, respectively) on the relaxed Ni_{55} cluster. C adsorption at the μ_6-sub site has the highest adsorption energy of 7.41 eV among all subsurface and surface adsorption sites on Ni_{55}. The μ_4-hol site is of comparable stability as the μ_6-sub site, and its adsorption energy is only 0.07 eV lower than that of the μ_6-sub site.

At the subsurface μ_6-sub sites, the interatomic distances between adsorbed C atoms and their nearest-neighbor Ni atoms ($R_{C–Ni}$) increase considerably (between 5 and 21%) compared to those at the surface sites. This interatomic distance expansion can be explained by the relief of the repulsive interaction between subsurface C atoms and their adjacent Ni atoms inside clusters [48]. We have further investigated the local charge variation upon C adsorption. We found that C atoms adsorbed at subsurface adsorption sites with a coordination of six Ni atoms possess a charge of about −1.10 e, higher than the charge of C atoms at any surface sites. It suggests a stronger C–Ni interaction when C atoms locate at subsurface sites.

Our results indicated that C atoms located at subsurface sites of Ni clusters are more stable than those on the surface sites. The next step is to find out whether a C atom can migrate directly from surface sites to subsurface sites? The PEP method described in the methodology session was first applied to investigate this problem. The curve in Fig. 3 depicted the potential energy profile for the diffusion of single C atom from the surface μ_3-fcc site to the subsurface μ_6-sub site in the relaxed Ni_{38} cluster. The calculated activation barrier is 0.26 eV. To validate the transition state found by the PEP method, the precise NEB method was also applied to locate the transition-state structure for the surface-to-subsurface C diffusion. The activation barrier (0.25 eV) obtained by the NEB method is only less 0.01 eV than that by the PEP method. In addition, the transition-state geometric structures from the two methods are very similar. As illustrated in Fig. 3, the PEP method shows that the distances between the C atom and Ni atoms are 1.72 and 1.75 Å, while the NEB method indicates the distances are 1.75 and 1.93 Å. The adsorbed C atom at the surface threefold μ_3-fcc site would break the longer Ni–Ni bond at one edge and interact with the forth Ni atom before it slips into the subsurface μ_6-sub site. Recently, Zhu et al. [24] reported that the activation barriers for C atom diffusion from surface threefold sites to subsurface sites were about 0.755 eV. Compared with their transition-state structures found on the periodic (111) slab surface, Ni atoms near the adsorbed C atom have a coordination number of 9. However, on our Ni_{38} cluster, Ni atoms adjacent to the carbon atom have smaller coordination numbers of 6 or 8. Thus, it is expected the C diffusion from the surface μ_3-fcc site to the subsurface μ_6-sub site on a Ni cluster would be easier than on a periodic slab. Vines et al. recently also reported a similar finding, that the C atom diffusion on Pb clusters from surface sites into tetrahedral subsurface sites is almost non-activated [49]. They have proposed that this is due to the high mobility of low-coordinated Pb atoms at cluster edges. These results resolve our puzzle, and we conclude that it is thermodynamically and kinetically feasible for a C atom adsorbed on Ni cluster surface to migrate into the underlying interstitial subsurface positions. This finding also supports the previous speculations that C atoms may enter the metal nanoclusters during CNT growth [9–11].

4 Conclusion

This study systematically investigated the adsorption energies of atomic carbon on Ni clusters with various cluster sizes (Ni_{13}, Ni_{15}, Ni_{38}, and Ni_{55}). On both fixed and relaxed clusters, C atom prefers to adsorb at high-coordination sites. μ_4-100 was found to be the most stable

adsorption site on the fixed Ni clusters. The μ_3-hcp and μ_3-fcc sites are of comparable stability, but less favored than the μ_4-100 site by ~ 0.8 eV. Taking cluster relaxation into account, new stable adsorption sites were found on the relaxed clusters. C atoms located at subsurface sites of Ni clusters are more stable than C atoms on the surface sites. Furthermore, the migration of surface C atom located on the threefold hollow site into the underlying interstitial subsurface positions is thermodynamically and kinetically feasible. These results indicate that CNT growth would involve both surface and subsurface C atoms coupled with surface reconstruction of Ni nanoclusters. Our results highlight that C diffusion and CNT cap formation need to be investigated on relaxed clusters for a better understanding of CNT growth mechanism.

References

1. Jorio A, Dresselhaus G, Dresselhaus MS (2008) Carbon nanotubes, advanced topics in the synthesis, structure, properties and applications. Springer, Berlin
2. Joselevich E, Dai HJ, Liu J, Hata KJ, Windle AH (2008) In: Jorio A, Dresselhaus G, Dresselhaus MS (eds) Carbon nanotubes, advanced topics in the synthesis, structure, properties and applications. Springer, Berlin
3. Iijima S, Ichihashi T (1993) Nature 363:603
4. Thess A, Lee R, Nikolaev P, Dai HJ, Petit P, Robert J, Xu CH, Lee YH, Kim SG, Rinzler AG, Colbert DT, Scuseria GE, Tomanek D, Fischer JE, Smalley RE (1996) Science 273:483
5. Journet C, Maser WK, Bernier P, Loiseau A, delaChapelle ML, Lefrant S, Deniard P, Lee R, Fischer JE (1997) Nature 388:756
6. Bandow S, Asaka S, Saito Y, Rao AM, Grigorian L, Richter E, Eklund PC (1998) Phys Rev Lett 80:3779
7. Kong J, Cassell AM, Dai HJ (1998) Chem Phys Lett 292:567
8. Cassell AM, Raymakers JA, Kong J, Dai HJ (1999) J Physl Chem B 103:6484
9. Kanzow H, Ding A (1999) Phys Rev B 60:11180
10. Gavillet J, Loiseau A, Journet C, Willaime F, Ducastelle F, Charlier JC (2001) Phys Rev Lett 87:275504
11. Harutyunyan AR, Awasthi N, Jiang A, Setyawan W, Mora E, Tokune T, Bolton K, Curtarolo S (2008) Phys Rev Lett 100:195502
12. Shibuta Y, Maruyama S (2003) Chem Phys Lett 382:381
13. Ding F, Rosen A, Bolton K (2004) J Chem Phys 121:2775
14. Reich S, Li L, Robertson J (2006) Chem Phys Lett 421:469
15. Li L, Reich S, Robertson J (2006) J Nanosci Nanotechnol 6:1290
16. Hofmann S, Sharma R, Ducati C, Du G, Mattevi C, Cepek C, Cantoro M, Pisana S, Parvez A, Cervantes-Sodi F, Ferrari AC, Dunin-Borkowski R, Lizzit S, Petaccia L, Goldoni A, Robertson J (2007) Nano Lett 7:602
17. Raty JY, Gygi F, Galli G (2005) Phys Rev Lett 95:096103
18. Muller JE, Wuttig M, Ibach H (1986) Phys Rev Lett 56:1583
19. Panas I, Schule J, Brandemark U, Siegbahn P, Wahlgren U (1988) J Phys Chem 92:3079
20. Fournier R, Andzelm J, Goursot A, Russo N, Salahub DR (1990) J Chem Phys 93:2919
21. Burghgraef H, Jansen APJ, Vansanten RA (1995) Surf Sci 324:345
22. Zhang QM, Wells JC, Gong XG, Zhang ZY (2004) Phys Rev B 69:205413
23. Xu J, Saeys M (2008) J Phys Chem C 112:9679
24. Zhu YA, Dai YC, Chen D, WK Y (2007) Surf Sci 601:1319
25. Zhu YA, Zhou XG, Chen D, Yuan WK (2007) J Phys Chem C 111:3447
26. Xiang Y, Sun DY, Gong XG (2000) J Phys Chem A 104:2746
27. Kilcoyne ALD, Woodruff DP, Robinson AW, Lindner Th, Somers JS, Bradshaw AM (1991) Surf Sci 253:107
28. Jónsson H, Mills G, Jacobsen KW (1998) Nudged elastic band method for finding minimum energy paths of transitions. In: Berne BJ, Ciccotti G, Coker DF (eds) Classical and quantum dynamics in condensed phase simulations, World Scientific, Singapore, P 385
29. Perdew JP, Burke K, Ernzerhof M (1996) Phys Rev Lett 77:3865
30. Kresse G, Furthmuller J (1996) Comput Mater Sci 6:15
31. Kresse G, Furthmuller J (1996) Phys Rev B 54:11169
32. Blöhl PE (1994) Phys Rev B 50:17953
33. Kresse G, Joubert D (1999) Phys Rev B 59:1758
34. Reddy BV, Nayak SK, Khanna SN, Rao BK, Jena P (1998) J Phys Chem A 102:1748
35. Henkelman G, Arnaldsson A, Jonsson H (2006) Comput Mater Sci 36:354
36. Sanville E, Kenny SD, Smith R, Henkelman G (2007) J Comput Chem 28:899
37. Apra E, Fortunelli A (2003) J Phys Chem A 107:2934
38. Knickelbein MB (2001) J Chem Phys 115:5957
39. Apai G, Hamilton JF, Stohr J, Thompson A (1979) Phys Rev Lett 43:165
40. Chen ZX, Neyman KM, Lim KH, Rosch N (2004) Langmuir 20:8068
41. Lim KH, Neyman KM, Rosch N (2006) Chem Phys Lett 432:184
42. Li X, Wong MSM, Lim KH (2010) Theoret Chem Acc. doi: 10.1007/s00214-010-0728-4
43. Neyman KM, Inntam C, Gordienko AB, Yudanov IV, Rosch N (2005) J Chem Phys 122:4705
44. Bader M, Ocal C, Hillert B, Haase J, Bradshaw AM (1987) Phys Rev B 35:5900
45. Isett LC, Blakely JM (1975) Surf Sci 47:645
46. Isett LC, Blakely JM (1976) Surf Sci 58:397
47. Eizenberg M, Blakely JM (1979) Surf Sci 82:228
48. Yudanov IV, Neyman KM, Rosch N (2004) Phys Chem Chem Phys 6:116
49. Vines F, Loschen C, Illas F, Neyman KM (2009) J Catal 266:59–63